



**HAL**  
open science

## Applying geochemical and colour properties to quantify sediment sources in a Brazilian semiarid ephemeral river system

Rennan Cabral Nascimento, Angelo Jamil Maia, Ygor Jacques Agra Bezerra da Silva, Fábio Farias Amorim, Clístenes Williams Araújo Do Nascimento, Tales Tiecher, O. Evrard, Adrian L Collins, Caroline Miranda Biondi, Yuri Jacques Agra Bezerra da Silva

### ► To cite this version:

Rennan Cabral Nascimento, Angelo Jamil Maia, Ygor Jacques Agra Bezerra da Silva, Fábio Farias Amorim, Clístenes Williams Araújo Do Nascimento, et al.. Applying geochemical and colour properties to quantify sediment sources in a Brazilian semiarid ephemeral river system. *Journal of Hydrology*, 2022, 613 (Part A), pp.128360. 10.1016/j.jhydrol.2022.128360 . cea-03758934

**HAL Id: cea-03758934**

**<https://cea.hal.science/cea-03758934>**

Submitted on 23 Aug 2022

**HAL** is a multi-disciplinary open access archive for the deposit and dissemination of scientific research documents, whether they are published or not. The documents may come from teaching and research institutions in France or abroad, or from public or private research centers.

L'archive ouverte pluridisciplinaire **HAL**, est destinée au dépôt et à la diffusion de documents scientifiques de niveau recherche, publiés ou non, émanant des établissements d'enseignement et de recherche français ou étrangers, des laboratoires publics ou privés.

Copyright

1           **Applying geochemical and colour properties to quantify sediment sources in a**  
2                           **Brazilian semiarid ephemeral river system**

3   Rennan Cabral Nascimento<sup>a</sup>, Angelo Jamil Maia<sup>a</sup>, Ygor Jacques Agra Bezerra da Silva<sup>a</sup>, Fábio  
4   Farias Amorim<sup>a</sup>, Clístenes Williams Araújo do Nascimento<sup>a</sup>, Tales Tiecher<sup>b</sup>, Olivier Evrard<sup>c</sup>,  
5   Adrian L. Collins<sup>d</sup>, Caroline Miranda Biondi<sup>a</sup>, Yuri Jacques Agra Bezerra da Silva<sup>e</sup>

6  
7   <sup>a</sup>Agronomy Department, Federal Rural University of Pernambuco (UFRPE), Dom Manuel de Medeiros Street, s/n -  
8                           Dois Irmãos, 52171-900 Recife, PE, Brazil

9   <sup>b</sup>Department of Soil Science, Federal University of Rio Grande do Sul (UFRGS), Interdisciplinary Research Group  
10   on Environmental Biogeochemistry (IRGEB), Bento Gonçalves Ave. 7712, 91540-000 Porto Alegre, RS, Brazil

11   <sup>c</sup>Laboratoire des Sciences du Climat et de l'Environnement (LSCE/IPSL), Unité Mixte de Recherche 8212 (CEA-  
12                           CNRS-UVSQ), Université Paris-Saclay, Gif-sur-Yvette, France

13   <sup>d</sup>Net zero and resilient farming, Rothamsted Research, North Wyke, Okehampton EX20 2SB, UK

14   <sup>e</sup>Agronomy Department, Federal University of Piauí (UFPI), Planalto Horizonte, 64900-000 Bom Jesus, PI, Brazil  
15

16   **Abstract**

17   The Brazilian semiarid is the most densely populated dry region in the world. Although  
18   climate change projections underline the need for the creation of integrated strategies to  
19   protect water resources in the semiarid, sediment source apportionment data remain scant  
20   for this environment. Accordingly, we evaluated sediment source contributions in one of  
21   the most relevant Brazilian semiarid catchments by combining geochemical and colour  
22   tracer properties. In doing so, we explored the applicability of colour tracers as a low-cost  
23   alternative to the use of time-consuming and costly properties, such as geochemical  
24   tracers. Two source classification schemes were used based on environmentally  
25   contrasting regions within the catchment (upper, middle and lower catchment parts) and  
26   land use (Caatinga biome - natural vegetation, unpaved roads, and channel banks).  
27   Suspended sediments (SS) and bed sediments (BS) were used as target sediment. A total  
28   of 660 individual source material samples were collected and composited. Geochemical  
29   and colour tracers were measured on the source and target sediment samples and used as  
30   potential fingerprints to discriminate and quantify the sediment source contributions. The  
31   geochemical tracers provided weak source discrimination based on land use. However,  
32   combining geochemical and colour tracers improved the final outputs. Using the  
33   MixSIAR model, the lower catchment contributed more sediment than the other regional  
34   sources. The Caatinga (SS = 49%; BS = 47%) contributed more sediment than channel  
35   banks (SS = 35%; BS = 39%). Overall, our results suggest that the recovery and  
36   conservation of the Caatinga vegetation and the stabilization of channel banks, especially  
37   in the lower catchment part, are critical for improving sediment supply control in the

38 semiarid study basin. More studies are needed to evaluate the conservative behaviour of  
39 colour tracers in ephemeral rivers.

40

41 Keywords: Drylands; Sediment fingerprinting; Colour tracers; Soil erosion; Climate  
42 change; Sediment transport.

43

## 44 **1. Introduction**

45

46 Climate change projections underline the urgency of creating integrated strategies  
47 for protecting water resources and guaranteeing the continued development of dry regions  
48 (IPCC, 2014). In Brazil, the semiarid region, the most densely populated dry region in the  
49 world (Marengo, 2008), covers 982,563 km<sup>2</sup> of the country and is mainly concentrated in  
50 the Northeast region. The high spatial and temporal variability of rainfall and the high air  
51 temperatures and evapotranspiration rates have led to an historical problem of water  
52 availability in this region (Correia, 2011). These background problems draw attention to  
53 the necessity of tackling soil erosion and sediment transfer within semiarid catchments  
54 since the excessive accumulation of fine-grained sediment threatens water quality and  
55 decreases reservoir storage capacity (Ayrault et al., 2014; Simplício et al., 2020). In recent  
56 decades, the intense deforestation of native vegetation in Brazilian drylands, triggered by  
57 agricultural activities, overgrazing, and coal production, has led to an increase in soil  
58 erosion (Medeiros et al., 2014; Tomasella et al., 2018; Neto et al., 2020). Therefore,  
59 understanding sediment source apportionment at the catchment scale is crucial for  
60 implementing targeted strategies to control the transfer of sediments and associated  
61 pollutants to surface waters. The sediment fingerprinting approach has been the most  
62 widely used direct means of investigating sediment provenance (Collins et al., 2020).  
63 Although this approach has been successfully used in other Brazilian rivers in the  
64 subtropics (Minella et al., 2007; Tiecher et al., 2014; Ramon et al., 2020), its application  
65 for sediment source apportionment in a Brazilian semiarid ephemeral river system has  
66 not been reported yet, representing a significant research gap (Silva et al., 2018a; Collins  
67 et al., 2020).

68 Various properties have been used to achieve sediment source apportionment,  
69 such as geochemical elements (Collins et al., 1997; Batista et al. 2019), radionuclides  
70 (Walling and Woodward, 1992; Ben Slimane et al., 2016), C and N stable isotopes  
71 (Garzon-Garcia et al., 2017; Collins et al., 2019) and spectroscopic properties (Tiecher et

72 al., 2016; Amorim et al., 2021). However, the time and resources required to analyse  
73 some of these tracers frequently determine the tracer selection and the ongoing lack of  
74 standardization among source fingerprinting procedures continues to hinder the wider  
75 application of the fingerprinting approach around the world (Collins et al., 2020). For  
76 instance, the use of colour tracers is relatively simple, less time-consuming and associated  
77 with a lower cost than other properties. Accordingly, colour has been used as an  
78 alternative sediment source tracer in many catchments under humid climates (Martínez-  
79 carreras et al., 2010; Tiecher et al., 2015; Amorim et al., 2021; Pulley and Collins, 2021).  
80 In contrast, studies reporting the applicability of colour tracers in dry environments  
81 remain scarce for fluvial sediment fingerprinting and incipient for aeolian sediments  
82 (Pulley and Rowntree, 2016; Nosrati et al., 2020; Nosrati et al., 2021a).

83         The Ipojuca River is one of the most polluted catchments in Brazil and is largely  
84 (~70%) semiarid in nature. Sediment-associated metal concentrations and fluxes in this  
85 river are comparable to those observed in drainage systems heavily impacted by mining  
86 activities (Silva et al., 2015, 2018b). Bed sediments in the upper catchment (semiarid)  
87 exhibit, for instance, high levels of Ni and Zn (Silva et al., 2017). Battery factories, textile  
88 industries and some municipalities directly discharge non-treated wastewater into the  
89 main watercourse (Lima Barros et al., 2013). In the above context, the current research  
90 quantified source contributions to suspended sediments (SS) and bed sediments (BS)  
91 using geochemical and colour tracers in this semiarid catchment. In doing so, we explored  
92 the applicability of colour parameters as an alternative to geochemical tracers, which can  
93 be particularly problematic to use in catchments potentially impacted by substantial  
94 anthropogenic pollution.

## 95 **2. Material and methods**

### 96 **2.1 Study area**

97

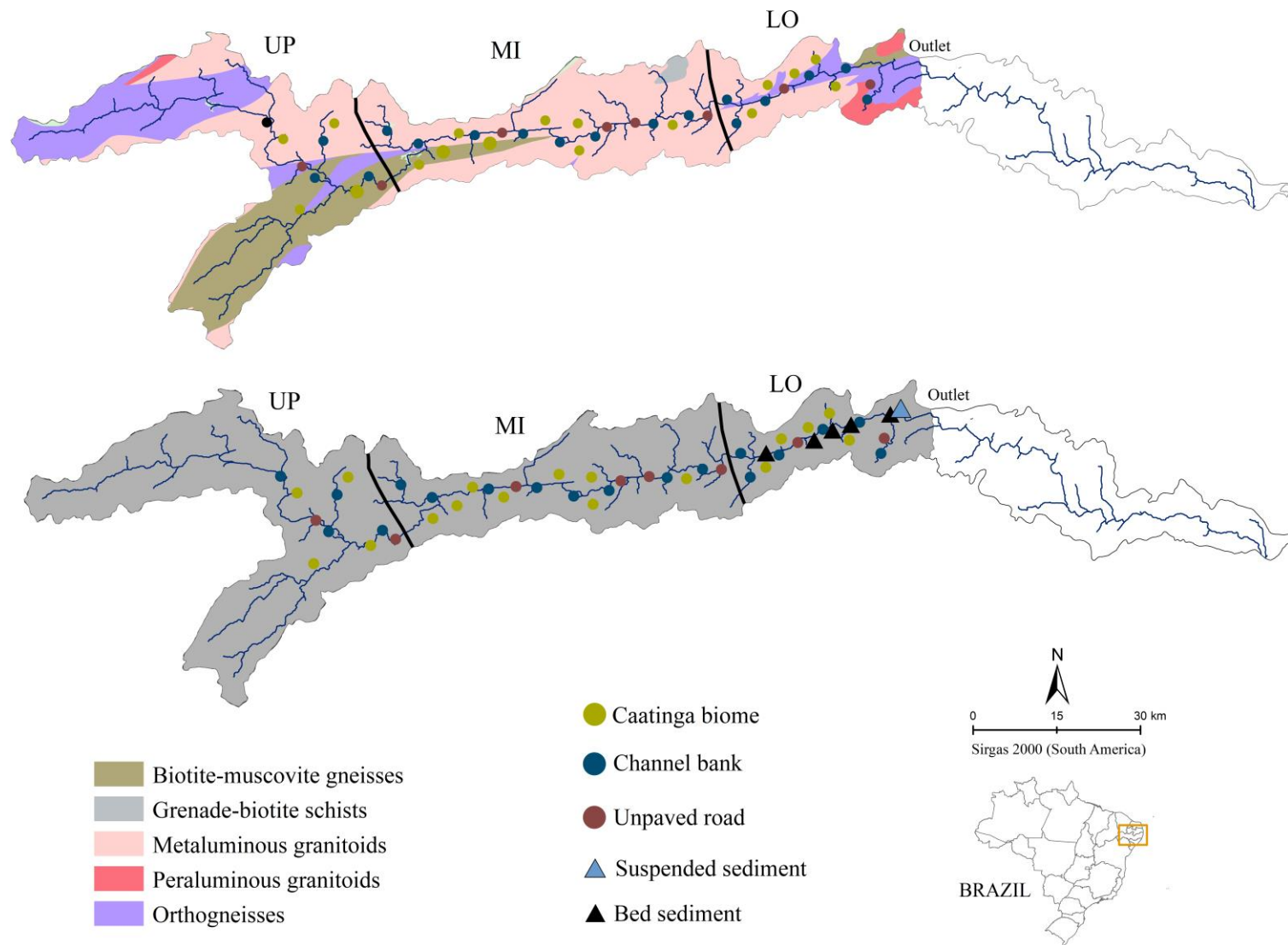
98         The semiarid part of the Ipojuca River basin (Figure 1) comprises an area of  
99 approximately 2500 km<sup>2</sup> (CONDEPE / FIDEM, 2005). The average annual rainfall ranges  
100 from 600 to 900 mm with high spatial and temporal variability, leading to an ephemeral  
101 and perennial fluvial regime in the upper and middle portions of the catchment,  
102 respectively (CONDEPE / FIDEM 2005). Soil parent materials are mainly metalluminous  
103 granitoids, orthogneisses and biotite-muscovite gneisses (Silva et al., 2015) (Figure 1).  
104 Soils are mostly Entisols, Alfisols, and Ultisols (CONDEPE / FIDEM 2005). The

105 preserved and semi-preserved areas of the Caatinga biome comprise a variety of  
106 vegetation species, such as *Mimosa tenuiflora* (Willd.)Poir., *Croton sonderianus* Muell.  
107 Arg, *Aspidosperma pyrifolium* Mart., *Combretum leprosum* Mart., *Cenostigma*  
108 *pyramidalis* E, Gagnon & GP Lewis, *Croton sonderianus* Muell. Arg, *Commiphora*  
109 *leptophloeos* (Mart.) JB Gillet, *Anadenanthera colubrina* (Vell.) Brenan, *Cereus*  
110 *jamacaru*, *Pilosocereus gounellei* and *Prosopis juliflora*. Many of these species have  
111 shrubby, thorny structures with twisted trunks and are predominantly hyperxerophilous  
112 (i.e., a group of species more resistant to aridity).

## 113 **2.2 Retrieval of source and target sediment samples**

114 Soil samples (see Figure 1) were collected from the main potential sediment  
115 sources. These sources were identified by a preliminary assessment of spatial  
116 representativeness using satellite images, soil, geology and slope maps. After that, a  
117 ground survey was performed to identify sampling locations hydrologically connected  
118 and delivering sediment directly to the main watercourse of the Ipojuca River and  
119 important tributaries. A total of 660 individual source samples were collected and  
120 composited into 44 source material samples. Each composite source sample was  
121 composed of 15 sub-samples collected at 0-5 cm depth for surface sources and from the  
122 lower horizons of channel bank profiles. Two source classification schemes were  
123 generated based on regional geological characteristics and land uses. The regional  
124 classification scheme assumed that different sources can be based on geological contrasts.  
125 Here, we divided the basin into three potential regional sources (Figure 1): upper (n =  
126 10), middle (n = 20), and lower (n = 14) catchment. The upper basin is represented  
127 geologically by Proterozoic volcano-sedimentary sequences, with a predominance of  
128 muscovite-biotite gneisses, metaluminous granitoids and metavolcanic rocks. The  
129 middle portion is underlain by a series of alkaline granitic rocks, such as alkali-feldspar  
130 granites, syenogranites, monzogranites, monzonites and quartzossienites. The lower  
131 basin is predominantly underlain by ortho-derivative gneisses (granodiorite and tonalite)  
132 containing amphibolite, migmatite, and metadiorite.

133 The source material samples were also classified according to land use (Figure 1):  
134 topsoils from the Caatinga biome (n = 17), channel banks (n = 20), and unpaved roads (n  
135 = 7). *Caatinga* samples represented the preserved and semi-preserved conditions found  
136 in the semiarid areas in the basin, and included samples collected under riparian  
137 vegetation.





139 **Fig. 1.** Location of the study catchment, geology and sampling sites for potential sediment source  
140 and target sediment samples. UP = upper catchment, MI = middle catchment, LO = lower  
141 catchment.

142  
143 Target suspended sediment samples (n = 3) were collected from a cross-section in  
144 the lowest reach of the study river using time-integrated samplers (Phillips et al., 2000).  
145 The suspended sediment samples collected represented material transiting in the river  
146 during the periods from May to June 2019 and from June to November 2019. These time  
147 periods represented the high and low water discharge periods, respectively. The total  
148 rainfall accumulation recorded during the entire observation period was 303 mm (Table  
149 S1), similar to the historical pattern observed during previous years in the region. Target  
150 bed sediment samples (n = 5) were collected by taking surface scrapes in November 2019  
151 in the lower catchment (Figure 1), exercising care not to exceed 5 cm in depth.

### 152 **2.3 Geochemical analyses**

153  
154 The source samples were air-dried whereas the target sediment samples were dried  
155 in a temperature-controlled circulation oven at 50 °C. All samples were passed through a  
156 32 µm mesh stainless steel sieve, the most important sediment size exported by the main  
157 watercourse (Fig. S1). Aliquots (0.5 g each) were first digested in 10 mL of HF in a resting  
158 system for 12 h. Subsequently, samples were digested in 5 mL of HNO<sub>3</sub> and 3 mL of  
159 HClO<sub>4</sub> at 180°C. This last process was repeated to ensure the complete digestion of the  
160 samples. Finally, the resulting extract was diluted in 5 mL of HCl (Estévez Alvarez et al.,  
161 2001). Standard operation and analytical data quality assurance procedures were  
162 followed, including the use of calibration curves, high purity acids, curve recalibration,  
163 analysis of reagent blanks, and standard reference materials (SRM 2709 Montana Soil,  
164 National Institute of Standards and Technology, NIST, 2002). All analyses were  
165 performed in duplicates. Total concentrations of Al, Ba, Ce, Co, Cr, Fe, La, Mn, Nd, Ni,  
166 Pb, Pr, Sc, Sm, Sn, Sr, Th, Ti, V, Y, Zn, and Zr were determined by ICP-OES (Optima  
167 DV7000, PerkinElmer). In order to improve the sensitivity to metal determination, we  
168 coupled a cyclonic spray chamber/nebulizer to the ICP-OES. Recovery rates ranged from  
169 83% to 106%. Total Zr concentrations were determined using portable X-ray fluorescence  
170 spectrometry (model S8 TIGER ECO - WDXRF-1KW).

171 Samples of granite, the most common rock type observed in the Ipojuca River  
172 catchment, were collected and the mineralogy analyzed on fine polished sections using a  
173 petrographic microscope (Murphy 1986). Mineral identification was carried out using a



174 scanning electron microscopy (SEM; TESCAN, VEGA-3 LMU) at an accelerating  
 175 voltage of 15 kV. Afterwards, an energy-dispersive X-ray spectroscopy (EDS) detector  
 176 (Oxford Instrument, model: 51-AD0007) coupled with SEM was used to determine the  
 177 elemental composition of the mineralogical assembly.

## 178 **2.4 Colour parameters**

179 The source material and target sediment samples were scanned using a  
 180 conventional office scanning system - EPSON EcoTank-L355 printer. RGB values were  
 181 averaged using the GIMP 2.10.22 software tools. Colosol software models (Viscarra  
 182 Rossel et al., 2004) were used to measure or calculate 24 colour parameters (table 1): Red  
 183 (R), Green (G), Blue (B), Hue ( $H_{col}$ ), Value ( $V_{col}$ ), Chroma ( $C_{col}$ ), Brightness ( $Y_{col}$ ),  
 184 Virtual component X (X), Virtual component Z (Z), Chromatic coordinate x (x),  
 185 Chromatic coordinate y (y), Dominant wavelength ( $\lambda_d$  (nm)), Purity of excitation (Pe),  
 186 Metric lightness function (L), Chromatic coordinate opponent red-green scales ( $a^*$ ),  
 187 Chromatic coordinate opponent blue-yellow scales ( $b^*$ ), Chromatic coordinate opponent  
 188 red-green scales ( $u^*$ ), Chromatic coordinate opponent blue-yellow scales ( $v^*$ ), CIE hue  
 189 ( $h^*$ ), CIE chroma ( $c^*$ ), Hue ( $H_{RGB}$ ), Light intensity ( $I_{RGB}$ ), Chromatic information ( $S_{RGB}$ ),  
 190 and Redness index (RI).

191 **Table 1.** Colour parameters used and their respective calculations used by the ColoSol  
 192 software.

Colour parameters	Calculation
Red (R)	direct measurement
Green (G)	direct measurement
Blue (B)	direct measurement
Hue ( $H_{RGB}$ )	$H_{RGB} = \frac{(2 \cdot G) - R - B}{R + G + B}$
Light intensity ( $I_{RGB}$ )	$I_{RGB} = \frac{R + G + B}{3}$
Chromatic information ( $S_{RGB}$ )	$S_{RGB} = \frac{R - B}{2}$
Chromatic coordinate x (x)	$x = \frac{X}{X + Y_{col} + Z}$
Chromatic coordinate y (y)	$y = \frac{Y_{col}}{X + Y_{col} + Z}$
Brightness ( $Y_{col}$ )	$Y_{col} = 11.396Y_c^{\frac{1}{3}} - 1.610$
Virtual component X (X)	$X = 11.559X_c^{\frac{1}{3}} - 1.695$
Virtual component Z (Z)	$Z = 11.510Z_c^{\frac{1}{3}} - 1.691$

Metric lightness function (L)	$L = 116 \cdot \left(\frac{Y_{col}}{Y_0}\right)^{\frac{1}{3}}$
Chromatic coordinate opponent red–green scales (u*)	$u^* = 13L \cdot (u' - u_n')$
Chromatic coordinate opponent blue–yellow scales (v*)	$v^* = 13L \cdot (v' - v_n')$
Chromatic coordinate opponent red–green scales (a*)	$a^* = 500 \cdot \left[ \left(\frac{X}{X_0}\right)^{\frac{1}{3}} - \left(\frac{Y_{col}}{Y_0}\right)^{\frac{1}{3}} \right]$
Chromatic coordinate opponent blue–yellow scales (b*)	$b^* = 500 \cdot \left[ \left(\frac{Y_{col}}{Y_0}\right)^{\frac{1}{3}} - \left(\frac{Z}{Z_0}\right)^{\frac{1}{3}} \right]$
CIE chroma (c*)	$c^* = \sqrt{(a^*)^2 + (b^*)^2}$
CIE hue (h*)	$h^* = \arctan\left(\frac{b^*}{a^*}\right)$
Hue (H <sub>col</sub> )	$H_{col} = \left  \tan^{-1}\left(\frac{S_2}{S_1}\right) \cdot \frac{100}{2\pi} \right $
Value (V <sub>col</sub> )	$V_{col} = f(Y)$
Chroma (C <sub>col</sub> )	$C_{col} = \sqrt{S_1^2 + S_2^2}$
Dominant wavelength (λ <sub>d</sub> (nm))	$P_e = \frac{x - x_w}{y - y_w}$
Purity of excitation (Pe)	$P_e = \frac{x - x_w}{y_b - y_w}$
Redness Index (RI)	$RI = \frac{L((a^*)^2 + (b^*)^2)^{0.5} \cdot 10^{8.2}}{b^* \cdot L^6}$

193

## 194 **2.5 Selection of tracers and apportionment of sediment sources**

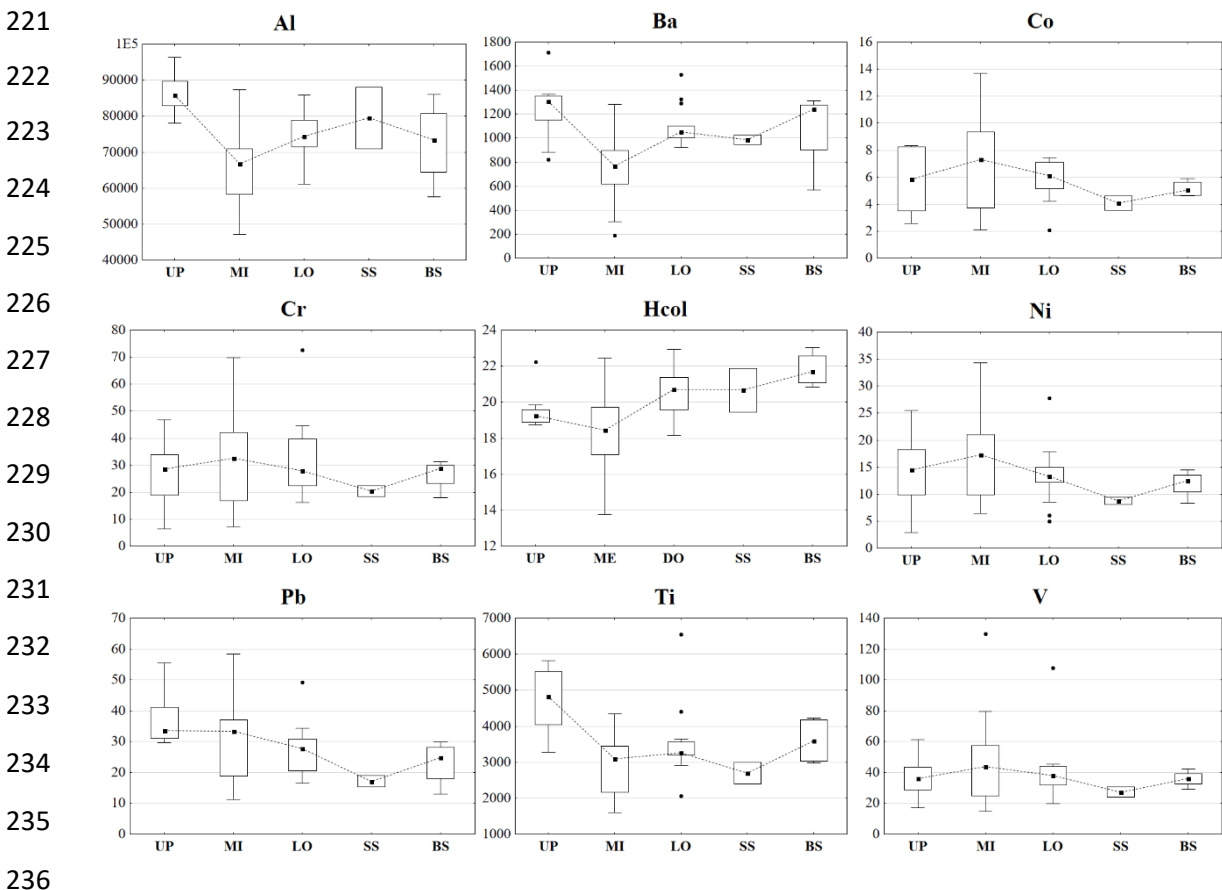
195 The selection of tracers for final composite fingerprints was undertaken using two  
196 steps: (1) assessment of conservative behaviour (i.e., range test), and; (2) linear  
197 discriminant function analysis (i.e., forward stepwise procedure). Conservation was  
198 tested by comparing the minimum and maximum values of the properties for source and  
199 target sediment samples, excluding outliers. Linear discriminant analysis ( $p < 0.1$ )  
200 selected the final set of tracers according to the minimization of Wilks' lambda. The  
201 MixSIAR model (Stock and Semmens, 2016) was used to estimate the mean relative  
202 source contributions. The Markov Chain Monte Carlo (MCMC) parameters in MixSIAR  
203 were set as follows: number of chains = 3; chain length = 100000; burn = 50000; thin =  
204 50. Model outputs were rejected if any variable was above 1.01 for Gelman-Rubin  
205 diagnostics. The model prediction accuracies were validated using virtual sediment  
206 mixtures, calculated as the product of the known contribution of each individual source  
207 and the corresponding average of the tracers measured in that source (Phillips and Gregg,  
208 2003). Here, the mean values of the root mean square error (RMSE) and mean absolute

209 error (MAE) were used as diagnostics for accuracy. All statistical procedures were  
210 performed using R software (version 3.6.1, R Core Team, 2021).

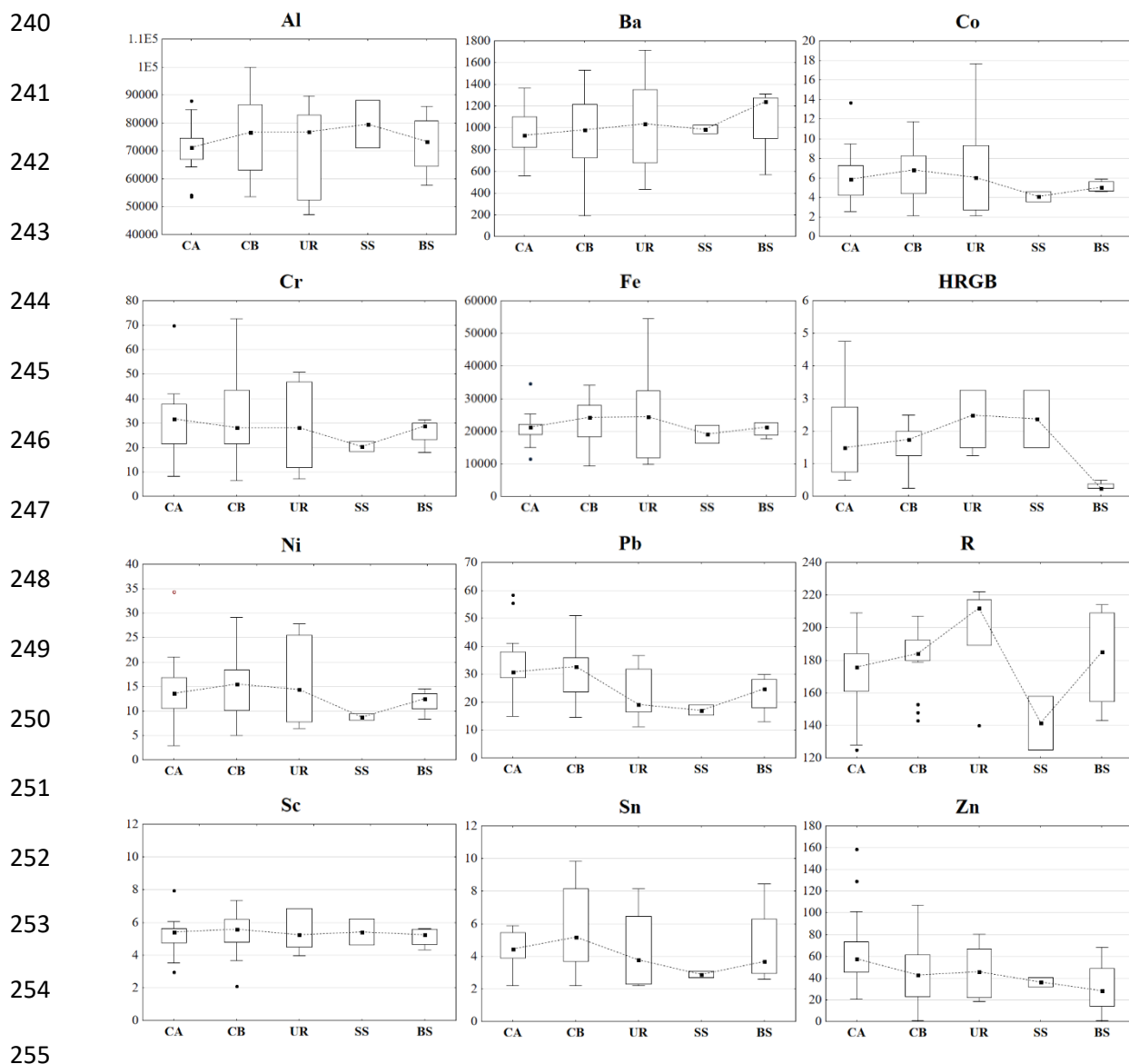
### 211 3. Results

#### 212 3.1 Selection of colour and geochemical tracers

213 The results of the range test for tracer conservation are presented in Figures 2 and  
214 3. Approximately 82% (regional sources) and 64% (land uses) of the geochemical  
215 elements passed this test. Non-conservative geochemical tracers were removed from the  
216 final discrimination and apportionment modelling for both regional sources (Ce, La, Th,  
217 and Zr) and land use sources (Ce, La, Nd, Pr, Sm, Y, Th, and Zr). Among the colour  
218 tracers, only  $H_{RGB}$ ,  $h^*$ ,  $H_{col}$  and  $\lambda_d$  (nm) for the regional sources and Red,  $H_{RGB}$ ,  $h^*$ ,  $H_{col}$ ,  
219 and  $\lambda_d$  (nm) for the land use sources passed the range test. Again, only those colour tracers  
220 passing the range test were included in the next steps of data processing.



237 **Fig. 2.** Boxplots of the geochemical ( $\text{mg kg}^{-1}$ ) and colour tracers passing the conservation test and  
238 using the regional sources classification scheme. UP = upper catchment, MI = middle catchment,  
239 LO = lower catchment; SS = target suspended sediments; BS = target bed sediments.



256 **Fig. 3.** Boxplots of geochemical ( $\text{mg kg}^{-1}$ ) and colour tracers passing the conservation test and  
 257 using the land use source classification scheme. CA = Caatinga; CB = channel banks; UR =  
 258 unpaved roads; SS = target suspended sediments; BS = target bed sediments.

259 The results of the forward stepwise LDA ( $p < 0.1$ ) for regional and land use sources  
 260 are shown in Tables 2 and 3, respectively. The geochemical tracers alone showed a higher  
 261 discriminatory power for regional sources (Figs. S2 and S3). The colour parameters alone  
 262 did not satisfy the minimum requirements for LDA (i.e., the number of approved variables  
 263 was lower than the number of potential sediment sources), selecting only  $H_{\text{col}}$  for both  
 264 source classification schemes, which provided a high percentage of discriminatory error:  
 265 Wilks' Lambda (WL) = 0.74 and Error rate (ER) = 0.40 (regional sources); WL = 0.78  
 266 and ER = 0.46 (land use sources). The final selected geochemical tracers (Ba, Cr, Ti, V,  
 267 Pb, and Ni) and the final combination of both types of tracers (Ba,  $H_{\text{col}}$ , Ti, Co, Ni, V, Cr,

268 Pb, and Al) were able to discriminate correctly 98% and 95% of the samples for the  
 269 regional sediment sources (Table 2). For the land use sediment source classification  
 270 scheme, the geochemical tracers alone (Fe, Zn, Sn, Sc, Ni, Ba, Al, and Co) and the  
 271 combination of geochemical and colour tracers (Fe, RED, Ti, Al, Ba, H<sub>RGB</sub>, Co, Zn, Sn,  
 272 Sc, Cr, and Pb) correctly classified 82% and 95% of the source material samples,  
 273 respectively (Table 3).

274 **Table 2.** Final composite signatures selected by linear discriminant analysis and corresponding  
 275 statistical results for the regional sediment source classification scheme for the Ipojuca River  
 276 catchment.

Tracers	Wilks' lambda	F-value	p-value	p-value (individual)	ER
Geochemical tracers					
Ba	0.50	20.30	<0.01	0.01	0.25
Cr	0.39	11.92	<0.01	0.01	0.18
Ti	0.23	14.17	<0.01	0.01	0.16
V	0.17	13.41	<0.01	0.01	0.11
Pb	0.15	12.02	<0.01	0.04	0.09
Ni	0.10	12.54	<0.01	0.00	0.02
Geochemical tracers + colour tracers					
Ba	0.50	20.30	<0.01	0.01	0.25
H <sub>col</sub>	0.39	12.22	<0.01	0.01	0.20
Ti	0.30	10.80	<0.01	0.01	0.20
Co	0.15	15.20	<0.01	0.01	0.11
Ni	0.13	13.37	<0.01	0.06	0.07
V	0.10	12.53	<0.01	0.03	0.07
Cr	0.09	11.88	<0.01	0.04	0.05
Pb	0.07	11.56	<0.01	0.04	0.02
Al	0.06	11.15	<0.01	0.06	0.05

277 ER = error rate; H<sub>col</sub> (Hue).

278

279

280

281 **Table 3.** Final composite signatures selected by linear discriminant analysis and corresponding  
 282 statistical results for the land use sediment source classification scheme for the Ipojuca River  
 283 catchment.

Tracers	Wilks' lambda	F-value	p-value	p-value (Individual)	ER
Geochemical elements					
Fe	0.85	3.48	0.04	0.04	0.45
Zn	0.72	3.55	0.01	0.03	0.34
Sn	0.63	3.37	0.01	0.07	0.30
Sc	0.56	3.19	0.01	0.10	0.32
Ni	0.45	3.68	0.01	0.01	0.25
Ba	0.39	3.64	0.01	0.08	0.27
Al	0.31	4.04	0.01	0.02	0.20
Co	0.26	4.05	0.01	0.07	0.18
Geochemical tracers + colour tracers					
Fe	0.85	3.48	3.48	0.04	0.45
RED	0.65	4.88	6.47	<0.01	0.36
Ti	0.52	5.11	4.93	0.01	0.34
Al	0.46	4.57	2.48	0.10	0.32
Ba	0.36	4.94	4.95	0.01	0.32
H <sub>RGB</sub>	0.29	5.17	4.46	0.02	0.16
Co	0.25	5.01	2.73	0.08	0.14
Zn	0.22	4.90	2.66	0.08	0.14
Sn	0.17	5.26	4.59	0.02	0.11
Sc	0.14	5.47	3.83	0.03	0.05
Cr	0.11	5.51	2.91	0.07	0.07
Pb	0.09	5.49	2.58	0.09	0.05

284 ER = error rate.

285

286

287

288

289

290

291 **3.2 Sediment source contributions and prediction uncertainties**

292 The average contributions of the regional sources to the two types of target  
293 sediment (i.e., SS and BS) were similar, regardless of the tracer set used (Figure 4) and  
294 followed the subsequent decreasing contribution order: lower catchment (LO) > upper  
295 catchment (UP) > middle catchment (MI). The lower sites showed higher contributions  
296 to SS and BS than the middle and upper catchment. Geochemically speaking, the Caatinga  
297 was the main land use-based sediment source (SS = 55% and BS = 54%). When using a  
298 combination of geochemical and colour tracers, the channel banks (SS = 40% and BS =  
299 45%) and Caatinga (SS = 43% and BS = 41%) showed relatively similar sediment  
300 contributions. The middle portion of the study basin and unpaved roads exhibited lower  
301 contributions to both SS and BS.

302

303

304

305

306

307

308

309

310

311

312

313

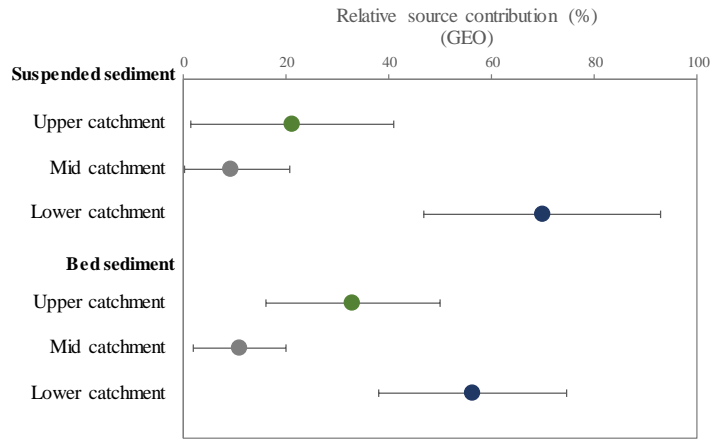
314

315

316

317

318



319

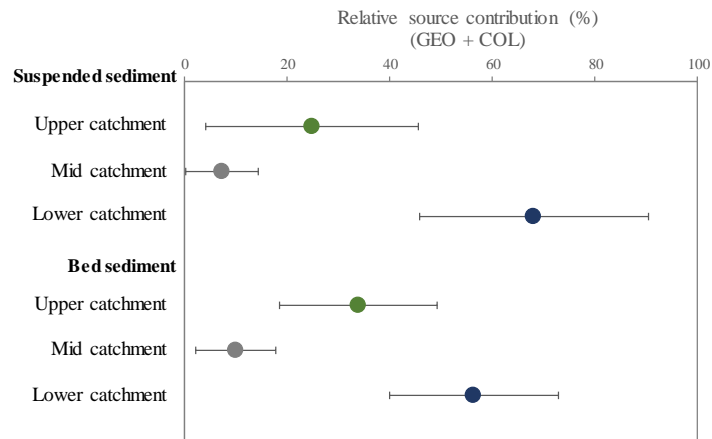
320

321

322

323

324



325

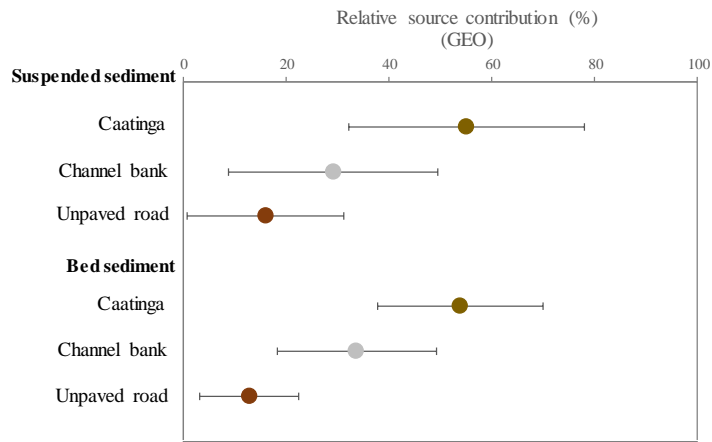
326

327

328

329

330



331

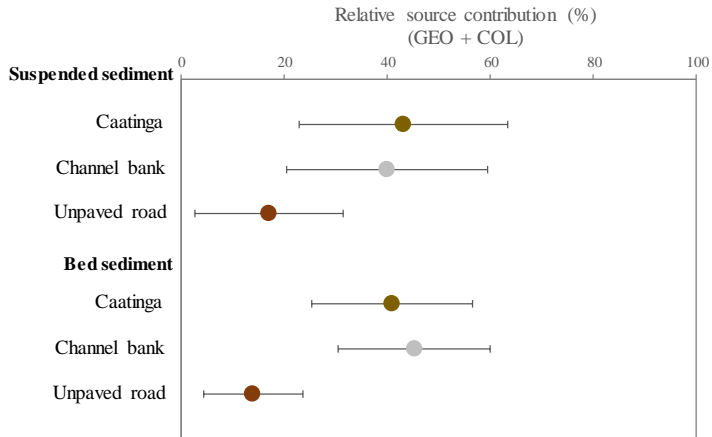
332

333

334

335

336



337

338

339

340



341 **Fig. 4.** Mean values and standard deviations for the predicted relative contributions to target  
 342 suspended sediments and bed sediments using the regional source and land use source  
 343 classification schemes. GEO = geochemical tracers; GEO + COL = geochemical + colour tracers.

344 The MixSIAR models used to estimate the sediment source contributions  
 345 exhibited convergence for the Gelman-Rubin test (<1.01) and sufficiently long Markov  
 346 chains. The low values for RMSE and MAE indicated that the predicted values were  
 347 similar to the known virtual mixtures. Therefore, all the modelled source contributions  
 348 were considered to be acceptably accurate (Table 4). The overall average values of RMSE  
 349 and MAE were 6.0% and 5.5%, respectively, and these are clearly comparable to the  
 350 accuracy reported by other studies using sediment source fingerprinting (Uber et al.,  
 351 2019; Nosrati et al., 2021b; Nosrati et al., 2021c; Amorim et al., 2021).

352 **Table 4.** Mean known and predicted relative contributions (and corresponding standard  
 353 deviations) of the sediment sources to target suspended sediment (SS) and bed sediment (BS)  
 354 samples and associated accuracies based on the virtual mixture tests.

Sources	Tracers	Target Sediment	Sources	Known mean contribution (%)	SD (%)	Predicted mean contribution (%)	RMSE	MAE
Regional	GEO	SS	UP	21.1	19.8	27.5	7.4	7.0
			MI	9.1	11.6	13.2		
			LO	69.8	23	59.4		
		BS	UP	32.9	16.9	34.8	4.5	4.2
			MI	10.8	9	15.2		
			LO	56.3	18.3	50.1		
	GEO + COL	SS	UP	24.8	20.7	22.7	3.2	3.0
			MI	7.2	8.3	11.7		
			LO	68	22.3	65.6		
		BS	UP	33.8	15.3	24.9	6.6	5.9
			MI	9.9	7.7	11.8		
			LO	56.3	16.4	63.3		
Use	GEO	SS	CA	55	23	46.8	10.3	9.7
			CB	29.1	20.3	43.7		
			UR	15.9	15.2	9.5		
		BS	CA	53.7	16.1	46.5	8.1	7.6
			CB	33.6	15.5	44.9		
			UR	12.8	9.6	8.6		
	GEO + COL	SS	CA	43.1	20.2	34.5	8.1	7.3
			CB	39.9	19.4	50.8		
			UR	17	14.4	14.6		

	CA	40.9	15.6	32.8		
BS	CB	45.2	14.7	52.6	6.3	5.4
	UR	13.9	9.6	14.6		

355

356 GEO = geochemical tracers; GEO + COL = geochemical + colour tracers; UP = upper catchment; MI =  
 357 middle catchment; LO = lower catchment; CA = Caatinga; CB = channel banks; UR = unpaved roads;  
 358 standard deviation (SD); root mean squared error (RMSE) and mean absolute error (MAE).

#### 359 **4. Discussion**

##### 360 ***4.1 Discrimination of regional sources and land uses***

361 In general, the geochemical tracers propagated lower errors for sediment source  
 362 discrimination and apportionment. This was most notable for the regional sediment  
 363 source scheme and possibly reflects the exclusive geochemical properties for each part of  
 364 the study catchment. The average Al, Ba, and Ti concentrations showed the main  
 365 contrasts between these sources and followed typically the sequence: upper catchment >  
 366 lower catchment > middle catchment. In the middle portion of the study catchment, the  
 367 lower Al contents were likely related to the predominance of metalluminous granitoids  
 368 containing a higher proportion of alkali metals (Figure 5b) in comparison to soils derived  
 369 from other parent materials (Figures 5a and 5c) (Table 5). The upper catchment exhibits  
 370 greater geological variation, including for instance the occurrence of orthogneisses,  
 371 volcano-sedimentary rocks, and intercalations of mafic rocks, mainly amphibolites. The  
 372 distribution of orthogneiss and volcano-sedimentary rocks are likely responsible for the  
 373 highest concentrations of Al, Ba, and Ti in the upper catchment. The lower catchment is  
 374 characterized by orthogneiss with different compositions, such as monzogranitic and  
 375 granodioritic.

376

377

378

379

380

381

382

383

384

385

386

387

388

389

390

391

392

393

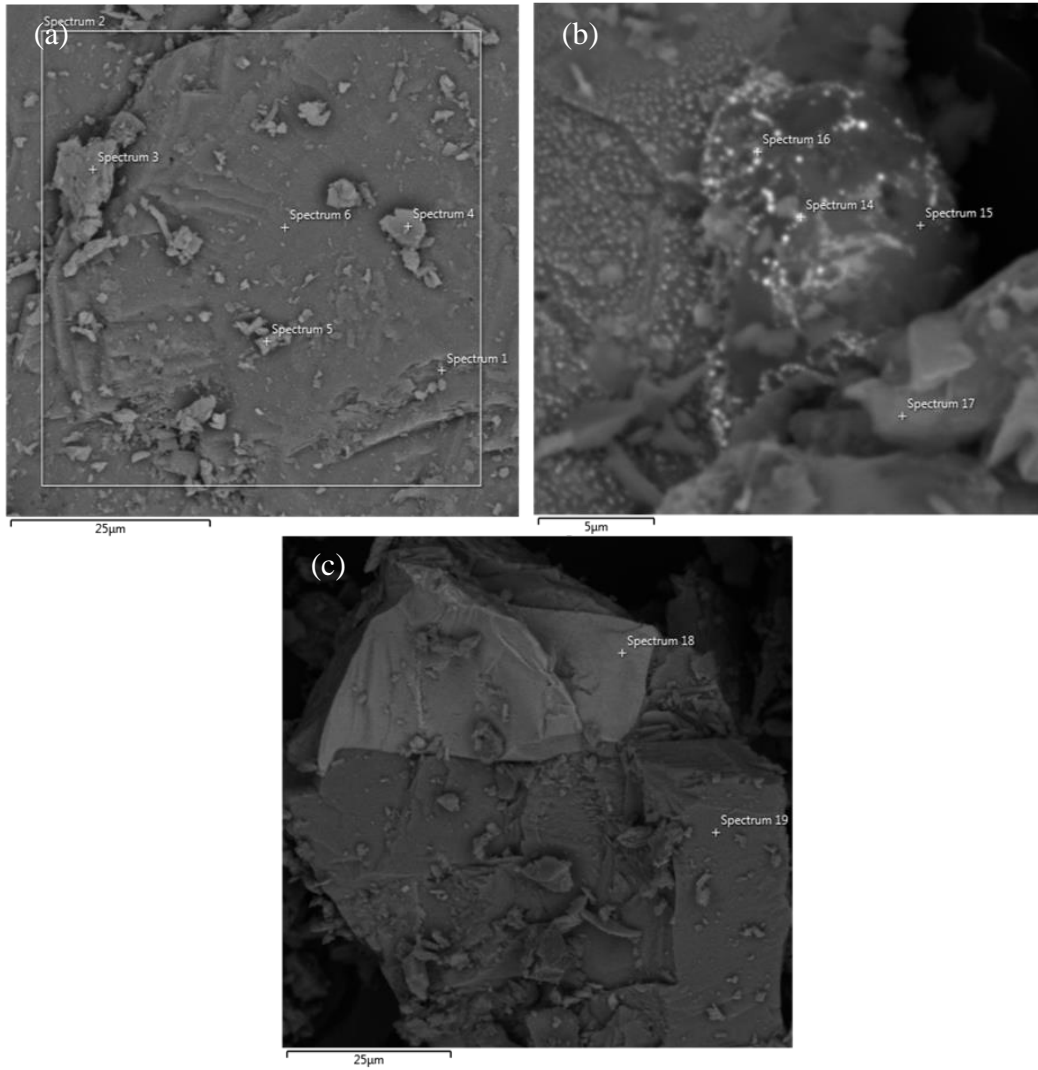
394

395

396

397

398



399

400

401

402

403

404

405

406

407

**Fig. 5.** Cross-sectional images of granites from the Ipojuca River basin using a scanning electron microscope with energy-dispersive X-ray spectroscopy attached facilities (SEMEDS). A) granite from the upper catchment. B) metaluminous granite from the middle catchment. C) granite from the upper catchment.

408 **Table 5.** Elemental composition of minerals in granites in the Ipojuca River watershed, using a  
 409 scanning electron microscope with energy-dispersive X-ray spectroscopy attached facilities  
 410 (SEM-EDS).

Elements	C	O	Na	Mg	Al	Si	K	Ca	Fe	Ba
Granite from the upper catchment (a) (%)										
Spectrum 1		43.7	0.9		9.4	27.7	10.8		0.4	0.5
Metaluminous granite from the mid catchment (b) (%)										
Spectrum 14		22.3		2.2	3.3	7.3	3.6		4.9	
Spectrum 15	7.9	21.4	0.5	2.2	6.0	17.5	12.6	1.4	25.7	
Spectrum 16	6.4	25.7	1.0	1.8	5.6	16.3	9.9	1.1	16.7	
Spectrum 17	15.7	34.4	0.9	3.0	5.4	12.3	5.6	0.5	13.9	
Granite from the upper catchment (c) (%)										
Spectrum 19			1.7	11.2	9.6	39.4	1.5		22.5	

411

412 Unlike the geochemical tracers, the colour parameters showed poor conservative  
 413 behaviour (82% failed the range test). The high input of organic waste observed in the  
 414 Ipojuca River basin (Lima Barros et al., 2013) and the particle size fraction used (<32  
 415  $\mu\text{m}$ ) might have combined via the enrichment of sediment in organic matter to reduce the  
 416 discriminatory efficiency of colour parameters (Pulley and Rowntree, 2016; Pulley and  
 417 Collins, 2022). When combined with geochemical parameters and following the land use  
 418 source classification scheme, RED and  $H_{\text{RGB}}$  exhibited significant variability and this was  
 419 fundamental in achieving more reliable source discrimination, increasing by 17% and  
 420 13%, the respective values of Wilks' Lambda and the samples correctly classified by  
 421 LDA. Unlike soils under natural vegetation in humid and cold environments, soils under  
 422 Caatinga did not show colour indices associated with darker shades. Most species of this  
 423 vegetation lose their leaves during a significant part of the year, mainly at the end of the  
 424 rainy season and at the beginning of the dry season. However, these climatic conditions,  
 425 and especially temperature and relative humidity, do not facilitate the accumulation of  
 426 organic matter in these soils (Costa et al., 2010; Lima et al., 2015; Holanda et al., 2017).  
 427 The rotation with agricultural activities, mainly agropastoral, and the lower biomass  
 428 production of mostly xerophytic species, compared to natural wetland species, may also  
 429 be responsible for this pattern (Almagro et al., 2015; Wiesmeier et al., 2019).

430

431

## 432 **4.2 Sediment source contribution patterns under semiarid environmental conditions**

433 The lower catchment contributed most of the sediment to the outlet of the  
434 investigated river system; approximately 69% and 56% of SS and BS, respectively. Low  
435 connectivity along the main stream may be responsible for promoting this pattern. Dams  
436 have been built over recent decades, modifying the dynamics of sediment redistribution  
437 and longitudinal connectivity (CONDEPE / FIDEM, 2005). The different rainfall regimes  
438 may also contribute as the annual rainfall increases from the upper to lower catchment  
439 (CONDEPE / FIDEM, 2005).

440 The average contributions of the upper catchment (SS = 23%; BS = 33%) were  
441 two-three fold greater than those estimated for the middle catchment (SS = 8%; BS =  
442 10%). Typically, sources collected at larger distances from target sediment collection  
443 points have lower contributions because of the longer travel pathways and times (Le gall  
444 et al., 2017; Silva et al., 2018a; Batista et al., 2019). Such effects are likely pronounced  
445 in our study basin due to the following reasons: 1) the presence of small dams; 2) the  
446 longer transport times in semiarid compared with humid environments, and; 3) the  
447 flattened shape of the basin. It is important to note that although the shape of the studied  
448 catchment results in a short distance from source to the main river channel, the lower  
449 rainfall regime in the upper part of the catchment may result in a longer period for the  
450 eroded soil particles reach the main river channel than in the lower portion of the  
451 catchment. Even though, some overestimation of the sediment contributions from the  
452 upper catchment may have occurred because of the close similarity of the geochemical  
453 properties of this zone with those found in the lower catchment, as observed for Co, Cr,  
454 Ni, and V and the corresponding LDA results (Figure 2). Gneisses and orthogneisses  
455 represent both of these two regions since they cover more than 62% of the upper  
456 catchment and almost all of the slope-channel connected areas in the lower catchment  
457 (Figure 1).

458 Overall, the Caatinga contribution (SS = 49%; BS = 47%) was slightly higher than  
459 that of channel banks (SS = 35%; BS = 39%) (Figure 4). Lower contributions from the  
460 Caatinga were expected here, due to its well-developed vegetation cover. On the one  
461 hand, in field experiments with simulated rainfall on soils under semiarid conditions, this  
462 vegetation type promoted similar or significantly lower rates of interrill erosion than areas  
463 under cultivation and bare soil (Cantalice et al., 2019; Cantalice et al., 2021). On the other  
464 hand, the combination of various factors may have contributed to our source

465 apportionment results: (1) the vegetation of the Caatinga biome covers the river basin  
466 almost entirely; also, it is often formed by secondary forest under initial or intermediate  
467 regeneration, characterized by shrubby plants with larger intervening spacing and during  
468 part of the year these plants lose their leaves reducing interception (Costa et al., 2010;  
469 Lima et al., 2015; Holanda et al., 2017; Menezes et al., 2021); (2) the rainfall in this region  
470 is typified by high-intensity regimes generating fast hydrological responses, minimizing  
471 the protection afforded by this type of native vegetation against erosion (Medeiros et al.,  
472 2014; Silva et al., 2015), and; (3) the widespread accumulation of sodium in soils may  
473 promote the dispersion of soil particles, thereby facilitating sediment mobilization in  
474 runoff (Souza et al., 2014).

475         The riparian vegetation does not protect channel banks sufficiently and did not  
476 result in low relative sediment contributions from channel banks (Silva et al., 2016; Devi  
477 et al., 2019). Here, channel banks correspond to deep walls incised by the river network,  
478 typically varying between 3-8 m in height. These morphological features can minimize  
479 root protection and lead to high erosion rates similar to degraded channel banks (Tiecher  
480 et al., 2018; Amorim et al., 2021). In contrast, unpaved roads were estimated to make  
481 lower contributions (SS = 16%; BS = 13%) to the sampled target sediment. The smaller  
482 relative area of unpaved road surfaces and their lower connectivity to the channel system  
483 may explain this result. Similarly, low sediment contributions from unpaved roads have  
484 also been reported for large river basins under humid climates (Tiecher et al., 2018;  
485 Ramon et al., 2020; Amorim et al., 2021).

## 486 **Conclusions**

487         The recovery and conservation of the vegetation in the Caatinga biome and the  
488 stabilization of channel banks, especially in the lower catchment, are fundamental to  
489 controlling the sediment problem in our semiarid study catchment. Poor conservative  
490 behaviour is one of the challenges for the application of colour tracers to quantifying  
491 sediment sources in this ephemeral river. Nevertheless, such tracers were fundamental for  
492 the most reliable sediment source apportionment based on the land use classification  
493 scheme. More studies are needed to evaluate the conservative behaviour of colour  
494 parameters in semiarid environments, especially at smaller scales. Sampling in smaller  
495 basins can better demonstrate sediment delivery dynamics within these environments  
496 since the transfer time of sediments is even longer in semiarid environmental conditions  
497 than in most humid conditions.

498 **Acknowledgements**

499 Y.J.A.B. Silva are grateful to the National Council for Scientific and Technological  
500 Development – CNPq for research productivity scholarships (Process Number:  
501 303221/2019-4). The contribution to this manuscript by ALC was funded by UKRI-  
502 BBSRC (UK Research and Innovation-Biotechnology and Biological Sciences Research  
503 Council) grant award BBS/E/C/000I0330.

504 **References**

505 Agência Condepe/Fidem, 2005. Rio Ipojuca, Recife. Série Bacias Hidrográficas de  
506 Pernambuco, 1.

507

508 Almagro, M., Maestre, F.T., Martínez-López, J., Valencia, E., Rey, A., 2015. Climate  
509 change may reduce litter decomposition while enhancing the contribution of  
510 photodegradation in dry perennial Mediterranean grasslands. *Soil. Biol. Biochem.* 90,  
511 214-223. <https://doi.org/10.1016/j.soilbio.2015.08.006>.

512

513 Amorim, F.F., da Silva, Y.J.A.B., Nascimento, R.C., da Silva, Y.J.A.B., Tiecher, T., do  
514 Nascimento, C.W.A., Minella, J.P.G., Zhang, Y., Ram, H.U., Pulley, S. Collins, A.L.,  
515 2021. Sediment source apportionment using optical property composite signatures in a  
516 rural catchment, Brazil. *Catena.* 202, 105208.  
517 <https://doi.org/10.1016/j.catena.2021.105208>.

518

519 Ayrault, S., Le Pape, P., Evrard, O., Priadi, C.R., Quantin, C., Bonté, P., Roy-Barman,  
520 M., 2014. Remanence of lead pollution in an urban river system: a multi-scale temporal  
521 and spatial study in the Seine River basin, France. *Environ. Sci. Pollut. R.* 21(6), 4134-  
522 4148. <https://doi.org/10.1007/s11356-013-2240-6>.

523

524 Batista, P.V., Laceby, J.P., Silva, M.L., Tassinari, D., Bispo, D.F., Curi, N., Davies, J.,  
525 Quinton, J.N., 2019. Using pedological knowledge to improve sediment source  
526 apportionment in tropical environments. *J. Soils Sediments.* 19(9), 3274-3289.  
527 <https://doi.org/10.1007/s11368-018-2199-5>.

528

529 Ben Slimane, A., Raclot, D., Evrard, O., Sanaa, M., Lefevre, I., Le Bissonnais, Y., 2016.  
530 Relative contribution of rill/interrill and gully/channel erosion to small reservoir siltation  
531 in Mediterranean environments. *Land Degrad. Dev.* 27 (3), 785-797.  
532 <https://doi.org/10.1002/ldr.2387>.

533

534 Cantalice, J.R.B., Nunes, E.O.S., Cavalcante, D.M., Barbosa, B., Junior, G.B., Guerra,  
535 S.M.S., Neto, F.R., 2019. Vegetative-hydraulic parameters generated by agricultural  
536 crops for laminar flows under a semi-arid environment of Pernambuco, Brazil. *Ecol.*  
537 *Indic.* 106, 105496. <https://doi.org/10.1016/j.ecolind.2019.105496>.

538

539 Cantalice, J.R.B., Dias, I.C.G.M., Andrade, D.S., Assis Filho, F.M., Souza, W.L.S.,  
540 Nunes, E.O.S., Junior, G.B., 2021. Hydraulic resistance to overland flow governed by  
541 Froude number on semiarid hillslopes under shrubs and crops. *Hydrolog. Sci. J.* 66(10)  
542 1531-1540, 2021. <https://doi.org/10.1080/02626667.2021.1947506>.

543

544 Collins, A.L., Walling, D.E., Leeks, G.J.L., 1997. Source type ascription for fluvial  
545 suspended sediment based on a quantitative composite fingerprinting technique. *Catena*.  
546 29(1), 1-27. [https://doi.org/10.1016/S0341-8162\(96\)00064-1](https://doi.org/10.1016/S0341-8162(96)00064-1).  
547

548 Collins, A.L., Burak, E., Harris, P., Pulley, S., Cardenas, L., Tang, Q., 2019. Field scale  
549 temporal and spatial variability of  $\delta^{13}\text{C}$ ,  $\delta^{15}\text{N}$ , TC and TN soil properties: implications  
550 for sediment source tracing. *Geoderma*. 333, 108-122.  
551 <https://doi.org/10.1016/j.geoderma.2018.07.019>.  
552

553 Collins, A.L., Blackwell, M., Boeckx, P., Chivers, C.A., Emelko, M., Evrard, O., Foster,  
554 I., Gellis, A., Gholami, H., Granger, S., Harris, P., Horowitz, A.J., Laceby, J.P., Martinez-  
555 carreras, N., Minella, J., Mol, L., Nosrati, K., Pulley, S., Silins, U., Silva, Y.J.A.B., Stone,  
556 M., Tiecher, T., Upadhayay, H.R., Zhang, Y., 2020. Sediment source fingerprinting:  
557 benchmarking recent outputs, remaining challenges and emerging themes. *J. Soils*  
558 *Sediments*. 20(12), 4160-4193. <https://doi.org/10.1007/s11368-020-02755-4>.  
559

560 Costa, C.C.D.A., Camacho, R.G.V., Macedo, I.D.D., Silva, P.C.M.D., 2010. Análise  
561 comparativa da produção de serapilheira em fragmentos arbóreos e arbustivos em área de  
562 caatinga na FLONA de Açú-RN. *Rev. Arvore*. 34, 259-265.  
563 <https://doi.org/10.1590/S0100-67622010000200008>.  
564

565 Devi, T.B., Sharma, A., Kumar, B., 2019. Flow characteristics in a partly vegetated  
566 channel with emergent vegetation and seepage. *Ecohydrol. Hydrobiol.* 19, 93-108.  
567 <https://doi.org/10.1016/j.ecohyd.2018.07.006>.  
568

569 Correia, R.C., Kiill, L.H.P., de Moura, M.S.B., Cunha, T.J.F., de Jesus Júnior, L.A.,  
570 Araújo, J.L.P., 2011. A região semiárida brasileira. Embrapa Semiárido-Capítulo em livro  
571 científico (ALICE).  
572

573 Estévez Alvarez, J., Montero, A., Jiménez, N., Muñoz, U., Padilla, A., Molina, R., Quicute  
574 de Vera, S., 2001. Nuclear and related analytical methods applied to the determination of  
575 Cr, Ni, Cu, Zn, Cd and Pb in a red ferralitic soil and Sorghum samples. *J. Radioanal.*  
576 *Nucl. Ch.* 247(3), 479-486. <https://doi.org/10.1023/a:1010640009301>.  
577

578 Garzon-Garcia, A., Laceby, J.P., Olley, J.M., Bunn, S.E., 2017. Differentiating the sources  
579 of fine sediment, organic matter and nitrogen in a subtropical Australian catchment. *Sci.*  
580 *Total Environ.* 575, 1384-1394. <https://doi.org/10.1016/j.scitotenv.2016.09.219>.  
581

582 Holanda, A.C.D., Feliciano, A.L.P., Freire, F.J., Sousa, F.Q.D., Freire, S.R.D.O., Alves,  
583 A.R., 2017. Aporte de serapilheira e nutrientes em uma área de caatinga. *Cienc. Florest.*  
584 27, 621-633. <https://doi.org/10.5902/1980509827747>.  
585

586 IPCC - Intergovernmental panel on climate change, 2014. *Climate Change 2014: Impacts,*  
587 *Adaptation, and Vulnerability.*  
588 [https://www.ipcc.ch/site/assets/uploads/2018/02/ar5\\_wgII\\_spm\\_en.pdf](https://www.ipcc.ch/site/assets/uploads/2018/02/ar5_wgII_spm_en.pdf). (accessed 2 May  
589 2021).  
590

591 Le Gall, M., Evrard, O., Dapoigny, A., Tiecher, T., Zafar, M., Minella, J.P.G., Laceby,  
592 J.P., Ayrault, S., 2017. Tracing sediment sources in a subtropical agricultural catchment



593 of Southern Brazil cultivated with conventional and conservation farming practices. *Land*  
594 *Degrad. Dev.* 28(4), 1426-1436. <https://doi.org/10.1002/ldr.2662>.  
595

596 Lima, R.P., Fernandes, M.M., Fernandes, M.R.D.M., Matricardi, E.A.T., 2015. Aporte e  
597 decomposição da serapilheira na Caatinga no Sul do Piauí. *Florest. Amb.* 22, 42-49, 2015.  
598 <https://doi.org/10.1590/2179-8087.062013>.  
599

600 Lima Barros, A.M., do Carmo Sobral M., Gunkel, G., 2013. Modelling of point and  
601 diffuse pollution: application of the Moneris model in the Ipojuca river basin,  
602 Pernambuco State, Brazil. *Wat. Sci. Tech.* 68(2), 357–365.  
603 <https://doi.org/10.2166/wst.2013.086>.  
604

605 Marengo, J.A., 2008. Vulnerabilidade, impactos e adaptação do clima no semiárido do  
606 Brasil. *Parcerias estratégicas*. Brasília, DF. N° 27,1-5.  
607

608 Martínez-Carreras, N., Udelhoven, T., Krein, A., Gallart, F., Iffly, J.F., Ziebel, J.,  
609 Hoffmann, L., Pfister, L., Walling, D.E., 2010. The use of sediment colour measured by  
610 diffuse reflectance spectrometry to determine sediment sources: application to the Atert  
611 River catchment (Luxembourg). *J Hydrol.* 382, 49-63..  
612 <https://doi.org/10.1016/j.jhydrol.2009.12.017>.  
613

614 Medeiros, P.H.A., de Araújo, J.C., 2014. Temporal variability of rainfall in a semiarid  
615 environment in Brazil and its effect on sediment transport processes. *J. Soils Sediments.*  
616 14(7), 1216-1223. <https://doi.org/10.1007/s11368-013-0809-9>.  
617

618 Menezes, R.S.C., Sales, A.T., Primo, D.C., de Albuquerque, E.R.G.M., de Jesus, K.N.,  
619 Pareyn, F.G.C., Sampaio, E.V.D.S.B., 2021. Soil and vegetation carbon stocks after land-  
620 use changes in a seasonally dry tropical forest. *Geoderma.* 390, 114943, 2021.  
621 <https://doi.org/10.1016/j.geoderma.2021.114943>.  
622

623 Minella, J.P.G., Merten, G.H., Reichert, J.M., Santos, D.R., 2017. Identificação e  
624 implicações para a conservação do solo das fontes de sedimentos em bacias hidrográficas.  
625 *Rev. Bras. Cienc. Solo.* v. 31, n. 6, p. 1637–1646, 2007. [https://doi.org/10.1590/S0100-](https://doi.org/10.1590/S0100-06832007000600039)  
626 [06832007000600039](https://doi.org/10.1590/S0100-06832007000600039).  
627

628 Murphy C.P., 1986. Thin section preparation of soils and sediments. Academic  
629 Publishing, Berkhamsterd (145 pp).  
630

631 NIST - National Institute of Standards and Technology, 2002. Standard Reference  
632 Materials -SRM 2709, 2710 and 2711.  
633

634 Neto, M.V.B.; de Araújo, M.D.S.B.; de Araújo Filho, J.C.; Sampaio, E.V.D.S.B.;  
635 Almeida, B.G., 2020. Rill and sheet soil erosion estimation in an area undergoing  
636 desertification in the Brazilian semi-arid region. *Model. Earth. Syst. Environ.* 1-9.  
637 <https://doi.org/10.1007/s40808-020-01026-y>.  
638

639 Nosrati, K., Akbari-Mahdiabad, M., Ayoubi, S., Degos, E., Koubansky, A., Coquatrix,  
640 Q., Collins, A. L. 2020. Storm dust source fingerprinting for different particle size  
641 fractions using colour and magnetic susceptibility and a Bayesian un-mixing model.

642 Environmental Environ. Sci. Pollut. R. 27(25), 31578-31594.  
643 <https://doi.org/10.1007/s11356-020-09249-3>.  
644

645 Nosrati, K., Akbari-Mahdiabad, M., Ayoubi, S., Collins, A. L. 2021a. An exploratory  
646 study on the use of different composite magnetic and colour fingerprints in aeolian  
647 sediment provenance fingerprinting. *Catena*. 200, 105182.  
648 <https://doi.org/10.1016/j.catena.2021.105182>.  
649

650 Nosrati, K., Akbari-Mahdiabad, M., Fiener, P., Collins, A.L., 2021b. Using different size  
651 fractions to source fingerprint fine-grained channel bed sediment in a large drainage basin  
652 in Iran. *Catena*. 200, 105173. <https://doi.org/10.1016/j.catena.2021.105173>.  
653

654 Nosrati, K., Mohammadi-Raigani, Z., Haddadchi, A., Collins, A. L., 2021c. Elucidating  
655 intra-storm variations in suspended sediment sources using a Bayesian fingerprinting  
656 approach. *J Hydrol*. 596, 126115. <https://doi.org/10.1016/j.jhydrol.2021.126115>.  
657

658 Phillips, J.M., Russell, M.A., Walling, D.E., 2000. Time-integrated sampling of fluvial  
659 suspended sediment: a simple methodology for small catchments. *Hydrol. Process*.  
660 14(14), 2589-2602. [https://doi.org/10.1002/1099-1085\(20001015\)14:14<2589::AID-  
661 HYP94>3.0.CO;2-D](https://doi.org/10.1002/1099-1085(20001015)14:14<2589::AID-HYP94>3.0.CO;2-D).  
662

663 Phillips, D.L., Gregg, J.W., 2003. Source partitioning using stable isotopes: coping with  
664 too many sources. *Oecologia*. 136(2), 261-269. [https://doi.org/10.1007/s00442-003-  
665 1218-3](https://doi.org/10.1007/s00442-003-1218-3).  
666

667 Pulley, S., Rowntree, K., 2016. The use of an ordinary colour scanner to fingerprint  
668 sediment sources in the South African Karoo. *J. Environ. Manage*. 165, 253-262.  
669 <https://doi.org/10.1016/j.jenvman.2015.09.037>.  
670

671 Pulley, S., Collins, A.L., 2021. The potential for colour to provide a robust alternative to  
672 high-cost sediment source fingerprinting: Assessment using eight catchments in England.  
673 *Sci. Total Environ*. 148416. <https://doi.org/10.1016/j.scitotenv.2021.148416>.  
674

675 Pulley, S., Collins, A.L. 2022. A rapid and inexpensive colour-based sediment tracing  
676 method incorporating hydrogen peroxide sample treatment as an alternative to  
677 quantitative source fingerprinting for catchment management. *J. Environ. Manage*. 311,  
678 114780. <https://doi.org/10.1016/j.jenvman.2022.114780>.  
679

680 Ramon, R., Evrard, O., Laceby, J.P., Caner, L., Inda, A.V., De Barros, C.A., Minella, J.  
681 P., Tiecher, T., 2020. Combining spectroscopy and magnetism with geochemical tracers  
682 to improve the discrimination of sediment sources in a homogeneous subtropical  
683 catchment. *Catena*. 195, 104800. <https://doi.org/10.1016/j.catena.2020.104800>.  
684

685 Silva, Y.J.A.B., Cantalice, J.R.B., Singh, V.P., do Nascimento, C.W.A., Piscocya, V. C.,  
686 Guerra, S.M., 2015. Trace element fluxes in sediments of an environmentally impacted  
687 river from a coastal zone of Brazil. *Environ. Sci. Pollut. R*. 22(19), 14755-14766.  
688 <https://doi.org/10.1007/s11356-015-4670-9>.  
689

690 Silva, Y.J.A.B., Cantalice, J.R.B., Singh, V.P., Cruz, C.M.C.A., da Silva Souza, W.L.,  
691 2016. Sediment transport under the presence and absence of emergent vegetation in a

692 natural alluvial channel from Brazil. *Int. J. Sediment. Res.* 31(4), 360-367.  
693 <https://doi.org/10.1016/j.ijsrc.2016.01.001>.  
694  
695 Silva, Y.J.A.B., Cantalice, J.R.B., do Nascimento, C.W.A., Singh, V.P., da Silva,  
696 Y.J.A.B., Silva, C.M.C.A.C., Silva, M.O., Guerra, S.M., 2017. Bedload as an indicator of  
697 heavy metal contamination in a Brazilian anthropized watershed. *Catena*. 153, 106-113.  
698 <https://doi.org/10.1016/j.catena.2017.02.004>.  
699  
700 Silva, E.M., Medeiros, P., Araújo, J.C.D., 2018a. Applicability of fingerprinting for  
701 identification of sediment sources in a mesoscale semiarid catchment. *Eng. Agric.* 38,  
702 553-562. <https://doi.org/10.1590/1809-4430-Eng.Agric.v38n4p553-562/2018>.  
703  
704 Silva, Y.J.A.B., do Nascimento, C.W.A, da Silva Y.J.A.B., Amorim, F.F., Cantalice,  
705 J.R.B., Singh, V.P., Collins, A.L., 2018b. Bed and suspended sediment-associated rare  
706 earth element concentrations and fluxes in a polluted Brazilian river system. *Environ. Sci.*  
707 *Pollut. R.* 25(34), 34426–34437. <https://doi.org/10.1007/s11356-018-3357-4>.  
708  
709 Simplício, A.A.F., Costa, C.A.G., Navarro-Hevia, J., de Araújo, J.C., 2020. Erosion at  
710 hillslope and micro-basin scales in the Gilbués Desertification Region, North-eastern  
711 Brazil. *Land Degrad. Dev.* <https://doi.org/10.1002/ldr.3809>.  
712  
713 Souza, E.R., dos Santos Freire, M.B.G., de Melo, D.V.M., de Assunção Montenegro,  
714 A.A., 2014. Management of *Atriplex nummularia* Lindl. in a salt affected soil in a semi  
715 arid region of Brazil. *Int. J. Phytoremediat.* 16(1), 73-85.  
716 <https://doi.org/10.1080/15226514.2012.759529>.  
717  
718 Stock, B.C., Semmens, B.X., 2016. *MixSIAR, G.U.I. User Manual. Version 3, 1.*  
719  
720 Tiecher, T., Minella, J.P.G., Miguel, P., Alvarez, J.W.R., Pellegrini, A., Capoane, V.,  
721 Ciotti, L.H., Schaefer, G.L., Santos, D.R.D., 2014. Contribuição das fontes de sedimentos  
722 em uma bacia hidrográfica agrícola sob plantio direto. *Rev. Bras. Cienc. Solo*, 38(2), 639-  
723 649. <https://doi.org/10.1590/S0100-06832014000200028>.  
724  
725 Tiecher, T., Caner, L., Minella, J.P.G., dos Santos, D.R., 2015. Combining visible-based-  
726 color parameters and geochemical tracers to improve sediment source discrimination and  
727 apportionment. *Sci. Total Environ.* 527, 135-149.  
728 <https://doi.org/10.1016/j.scitotenv.2015.04.103>.  
729  
730 Tiecher, T., Caner, L., Minella, J.P.G., Bender, M.A., dos Santos, D.R., 2016. Tracing  
731 sediment sources in a subtropical rural catchment of southern Brazil by using  
732 geochemical tracers and near-infrared spectroscopy. *Soil. Till. Res.* 155, 478-491.  
733 <https://doi.org/10.1016/j.still.2015.03.001>.  
734  
735 Tiecher, T., Minella, J.P.G., Evrard, O., Caner, L., Merten, G.H., Capoane, V., Didoné,  
736 E. J.; Dos Santos, D.R., 2018. Fingerprinting sediment sources in a large agricultural  
737 catchment under no-tillage in Southern Brazil (Conceição River). *Land Degrad. Dev.*  
738 29(4), 939-951. <https://doi.org/10.1002/ldr.2917>.  
739  
740 Tomasella, J., Vieira, R.M.S.P., Barbosa, A.A., Rodriguez, D.A., de Oliveira Santana,  
741 M., Sestini, M.F., 2018. Desertification trends in the Northeast of Brazil over the period

742 2000–2016. *Int. J. Appl. Earth Obs.* 73, 197-206.  
743 <https://doi.org/10.1016/j.jag.2018.06.012>.  
744  
745 Uber, M., Legout, C., Nord, G., Crouzet, C., Demory, F., Poulencard, J., 2019. Comparing  
746 alternative tracing measurements and mixing models to fingerprint suspended sediment  
747 sources in a mesoscale Mediterranean catchment. *J. Soils Sediments*. 1-19.  
748 <https://doi.org/10.1007/s11368-019-02270-1>.  
749  
750 Viscarra Rossel, R.A., 2004. ColoSol: executable software to perform colour space model  
751 transformations for soil colour.  
752  
753 Walling, D.E., Woodward, J.C., 1992. Use of radiometric fingerprints to derive  
754 information on suspended sediment sources. In *Erosion and sediment monitoring*  
755 *programmes in river basins*. Proc. international symposium, Oslo. (pp. 153-164).  
756 International Association of Hydrological Sciences.  
757  
758 Wiesmeier, M., Urbanski, L., Hobbey, E., Lang, B., Von Lützow, M., Marin-Spiotta, E.,  
759 Wesemael, B., Rabot, E., Ließ, M., Garcia-Franco, N., Wollschläger, U., Vogel, H.,  
760 Kögel-Knabner, I., 2019. Soil organic carbon storage as a key function of soils-A review  
761 of drivers and indicators at various scales. *Geoderma*. 333, 149-162.  
762 <https://doi.org/10.1016/j.geoderma.2018.07.026>.  
763